Mammogram Registration: A Phantom-Based Evaluation of Compressed Breast Thickness Variation Effects

Frédéric J. P. Richard, *Member, IEEE*, Predrag R. Bakić*, *Student Member, IEEE*, and Andrew D. A. Maidment, *Student Member, IEEE*

***Abstract*—The temporal comparison of mammograms is complex; a wide variety of factors can cause changes in image appearance. Mammogram registration is proposed as a method to reduce the effects of these changes and potentially to emphasize genuine alterations in breast tissue. Evaluation of such registration techniques is difficult since ground truth regarding breast deformations is not available in clinical mammograms. In this paper, we propose a systematic approach to evaluate sensitivity of registration methods to various types of changes in mammograms using synthetic breast images with known deformations. As a first step, images of the same simulated breasts with various amounts of simulated physical compression have been used to evaluate a previously described nonrigid mammogram registration technique. Registration performance is measured by calculating the average displacement error over a set of evaluation points identified in mammogram pairs. Applying appropriate thickness compensation and using a preferred order of the registered images, we obtained an average displacement error of 1.6 mm for mammograms with compression differences of 1–3 cm. The proposed methodology is applicable to analysis of other sources of mammogram differences and can be extended to the registration of multimodality breast data.**

***Index Terms*—Breast compression, evaluation, finite elements, image registration, mammogram synthesis, mammography, multigrid optimization, partial differential equations, tissue modeling.**

I. Introduction

RADIOLOGISTS analyze mammograms by examining temporal sequences of images. Such temporal comparisons have value because, to a first approximation, normal breasts do not change significantly over time, except for minor variations associated with the menstrual cycle or significant changes in body weight, [1], [2]. Some pathological changes in the breast are sufficiently subtle that they may pass unnoticed for many years; thus, radiologists compare images from a number of previous years. Such changes can be further obfuscated by different choices of X-ray technique, and variation in breast positioning or compression. It is our desire to develop methods which will increase the sensitivity to temporal pathological changes and develop means to evaluate these methods.

The task of comparing mammograms is difficult because there are many factors which may cause changes in image appearance, e.g., choice of image acquisition parameters, positioning and compression of the breast, image display parameters, and changes in breast anatomy. Changes such as those resulting from acquisition conditions tend to affect images globally and can typically be corrected by image normalization methods, [3]. Differences caused by changes in breast positioning and compression are more complex and more difficult to correct because mammograms are projections through the deformed breast. Mammogram registration is being considered as a method that could suppress technical variations (e.g., mammogram positioning and compression) and maintain or potentially emphasize genuine alterations in the breast, whether normal or abnormal.

This research was motivated in part by the development of systems for computer-aided diagnosis (CAD) of breast abnormalities, since some use bilateral or temporal mammogram comparisons to improve accuracy, [4]. As with clinical mammography, CAD systems are sensitive to various types of changes observed in mammograms. If not corrected, these normal changes generally decrease system performance by generating false-positive lesions or hiding true lesions. Therefore, registering mammograms is of importance for CAD system design.

More recently, both contrast-enhanced mammography [5], [6] and contrast-enhanced breast tomosynthesis [7] have been proposed. Both methods produce images of the breast in which the physiologic distribution of iodinated contrast agents is demonstrated. Two methods have been proposed [8]. Dual-energy subtraction [6] has the advantage that low- and high-energy images of the breast are acquired nearly simultaneously; thus, breast motion is minimized, but lesion contrast and background suppression is poor. Temporal subtraction [5] results in images with superior lesion contrast and background suppression, but are subject to motion artifacts. Accurate registration of precontrast and postcontrast images to compensate for any breast motion is, thus, essential.

Both rigid [9]–[12] and nonrigid [13]–[16] methods of mammogram registration have been proposed. No systematic evaluation of registration performance has been reported for specific

Manuscript received September 15, 2005; revised November 15, 2005. The Associate Editor responsible for coordinating the review of this paper and recommending its publication was N. Karssemeijer. *Asterisk indicates corresponding author.*

F. J. P. Richard is with the Department of Mathematics and Computer Science, University Paris 5-René Descartes, 75 270 Paris, cedex 06 France.

*P. R. Bakić is with the Department of Radiology, University of Pennsylvania, 3400 Spruce Street, Philadelphia, PA 19104 USA (e-mail: predrag.bakic@uphs.upemm.edu).

A. D. A. Maidment is with the Department of Radiology, University of Pennsylvania, Philadelphia, PA 19104 USA.

Digital Object Identifier 10.1109/TMI.2005.862204

causes of image variations. Such evaluations are difficult to implement using clinical data as images with known breast deformation and image acquisition differences do not exist.

Here, we present a systematic approach to evaluating the sensitivity of registration methods to various types of changes in mammograms. Although this paper focuses on an analysis of breast compression, the evaluation methodology described is also applicable to other sources of mammogram differences. The analysis is performed using synthetic images of the same simulated breasts with various amounts of breast compression. Modeling breast compression is a recent topic of research, [3], [17]–[19]. Use of synthetic images, if accurate enough, is advantageous as it allows precise control of breast deformation to be analyzed, provides knowledge of the ground truth of the breast anatomy before and after deformation, and enables variation in the composition of the breast; all without the need for additional exposures to volunteers.

II. Registration Method

Image registration involves finding correspondence between coordinates in an image pair. It is conventional to define the images on a continuous subset Ω of $\mathbb{R}^2$, [14], [20]–[22]. Image coordinates are matched via a function ϕ, which maps Ω onto itself. The composition of an image, I, and ϕ (denoted I_ϕ) is a geometric deformation of I. Registering two images I^0 and I^1 consists of finding a coordinate change ϕ, such that the deformed image I^0_ϕ is *similar* to the target image I^1, using appropriate criteria.

It is possible to formulate the image registration in terms of an inverse problem; namely, find a coordinate change ϕ belonging to a functional space $\mathcal{W}$ which minimizes an energy J_Ω composed of two terms

$$J_\Omega(\phi) = R_\Omega(\phi) + S_\Omega\left(I^0, I^1_\phi\right) \tag{1}$$

given specific boundary conditions. The first regularization term, $R_\Omega(\phi)$, is a smoothing term which ensures that the problem is well-posed and that solutions are nondegenerate and homeomorphic. The second similarity term, S_Ω, depends on image intensities. This term acts to constrain the registration by approaching a minimum when the deformed image I^1_ϕ and the target image I^0 are similar. Finally, we can use boundary conditions for the definition of additional registration constraints, [14]. The choice of appropriate similarity and regularization terms, and boundary conditions will determine the utility of the registration algorithm.

A. Regularization Term

Regularity constraints are usually derived from heuristic rules regarding geometric variations that one would expect to observe in images. For mammography we assume that variations can be characterized as elastic deformations. Hence, we define the regularization term as the strain energy of an elastic material. Following Ciarlet, [23], we define this strain energy as follows. Let A_Ω be the bilinear form defined for any $u, v \in \mathcal{W}$ as

$$A_\Omega(u,v) = \langle Lu, v\rangle_\Omega = \int_\Omega Lu(x)\cdot v(x)\,dx \tag{2}$$

where L is the operator of linearized elasticity

$$Lu = -\gamma\,\mathrm{div}\left\{\frac{\nu}{(1-\nu+2\nu^2)}\mathrm{tr}(\mathbf{e}(u))I_M + \frac{1}{1+\nu}(\mathbf{e}(u))\right\}. \tag{3}$$

The Young's modulus, γ, and Poisson ratio, ν, are positive coefficients, and $(\mathbf{e}(u))$ is the linearized strain tensor

$$\mathbf{e}(u) = \frac{1}{2}(\nabla u^T + \nabla u). \tag{4}$$

For a given 2×2-matrix $M, \mathrm{tr}(M)$ denotes the trace operator. For a given smooth function m, which maps Ω into the 2×2-matrix set, $\mathrm{div}\{m\}$ denotes the divergence operator. At a point x of $\Omega, \mathrm{div}\{m\}(x)$ is a two-dimensional (2-D) vector having the ith component equal to $\partial_{x_1} m(x)_{i1} + \partial_{x_2} m(x)_{i2}$. We denote by I_M the 2×2 identity matrix.

The regularization term is defined as

$$R_\Omega(\phi) = \frac{1}{2}A_\Omega(u,u) \tag{5}$$

where u are displacements associated with deformations ϕ ($\forall x \in \Omega, u(x) = \phi(x) - x$). In this expression, R_Ω can be factored by γ, so that this parameter should be interpreted as a weighting factor. Note that this value of γ is not derived from physical properties of the breast.

B. Similarity Criterion

The similarity criterion is used to account for pixel intensity differences between the images in a registration pair. We use a similarity criterion which is invariant to linear changes in image intensity, in the form $g_1 I + g_2$, where I is the analyzed image, and g_1 and g_2 are scalars. The invariance criterion is defined for all pairs of images (I, J) by

$$S_\Omega(I,J) = \frac{1}{2}\min_{(g_1,g_2)\in\mathbb{R}\times\mathbb{R}} |g_1 I + g_2 - J|^2_\Omega \tag{6}$$

which has a unique solution

$$\hat{g}_1(I,J) = \frac{\langle I - m_\Omega(I), J - m_\Omega(J)\rangle_\Omega}{|I - m_\Omega(I)|^2} \tag{7}$$

$$\hat{g}_2(I,J) = \frac{1}{|\Omega|}(m_\Omega(J) - \hat{g}_1 m_\Omega(I)) \tag{8}$$

where $m_\Omega(I)$ denotes $\int_\Omega I(x)\,dx$ and $\langle\cdot,\cdot\rangle_\Omega$ is the inner product defined for all I, J by $\int_\Omega I(x)J(x)\,dx$. Thus, the criterion can also be written as

$$S_\Omega(I,J) = |\hat{g}_1(I,J)I + \hat{g}_2(I,J) - J|^2_\Omega \tag{9}$$

the correlation ratio between images I and J.

C. Boundary Conditions

The registration constraints, as defined by the similarity term in (1), are based exclusively on image gray-levels. In breast imaging, however, it is also relevant to use breast borders as geometric constraints. The breast borders can usually act as a good initial registration.

The registration method described here combines intensity-based and border-based constraints. Let I^0 and I^1 be two mammograms to be registered. We assume that the locations of the breast borders are known in both images. We denote by Ω_0 and Ω_1 the set of breast coordinates in the respective mammograms. These sets are connected, open, and included in Ω. The boundaries of Ω_i are denoted by $\partial\Omega_i$ and their closures (which include both Ω_i and $\partial\Omega_i$) are denoted by $\bar{\Omega}_i$ $(i = 0, 1)$. The boundaries $\partial\Omega_i$ are the coordinates of the breast borders. We assume that a correspondence between boundaries was established in the initial registration, by matching the breast borders. Specifically, we locate breast contours in both images and then match contour points according to their relative positions in the contours, [14]. This correspondence is described by a function ϕ_0 (or $\mathrm{Id} + u_0$) which maps the coordinates of $\partial\Omega_0$ onto those of $\partial\Omega_1$.

By incorporating contour-based constraints in the registration method, the problem is restricted to the regions of interest (ROIs) Ω_0 and Ω_1. The image coordinate change ϕ is defined exclusively on these regions. More precisely, it is an element of a space $\mathcal{W}'$ composed of smooth functions mapping $\bar{\Omega}_0$ onto $\bar{\Omega}_1$. The inverse problem can then be stated as follows, [14].

Model 1: Find an element of $\mathcal{W}'$ which minimizes an energy J_{Ω_0} of the form

$$J_{\Omega_0}(u) = \frac{1}{2} A_{\Omega_0}(u, u) + S_{\Omega_0}\left(I^0, I^1_\phi\right) \tag{10}$$

with nonhomogeneous Dirichlet boundary conditions

$$\forall x \in \partial\Omega_0, \quad u(x) = u_0(x) = \phi_0(x) - x. \tag{11}$$

The energy terms of J_{Ω_0} have the same definitions and play the same roles as in (1), defined on the ROI Ω_0. The boundary conditions are additional registration constraints based on the breast borders as hard constraints, which are suitable whenever borders of the ROIs are segmented and matched accurately. When this is not the case, border-based constraints can be relaxed using free boundary conditions and extra energy terms, [14]. In order for the minimization problem in (10) to be defined and to have a solution, we have defined $\mathcal{W}'$ as the Sobolev space $H^1(\bar{\Omega}_0; \mathbb{R}^2)$. The choice of this Sobolev space ensures in particular that solutions are sufficiently differentiable. Appendix A describes a technique for numerical solution of this minimization problem.

III. Mammogram Simulation

We have applied the mammogram registration algorithm described in the previous section to registering images of the same breast taken with different amounts of mammographic compression. This problem regularly occurs in clinical cases, especially in breast cancer screening, since mammograms of the same woman taken at different times rarely have exactly the same compression and positioning. In this paper, we focus on registration of images acquired with different compressed breast thicknesses, assuming no other changes in breast composition or positioning between the two exams.

Obtaining clinical images of the same composition and with different compressed breast thicknesses is not a simple task. In screening, the breasts are imaged using a minimal number of views (typically either one or two views per breast) due to patient dose concerns. In addition, screening dates are separated temporally by one to two years on average; therefore, changes in breast composition may occur and positioning cannot be exactly replicated. In order to overcome these limitations, we have used synthetic mammograms generated by computer simulation of the mammographic acquisition using an anthropomorphic breast model, developed by Bakic *et al.*, [24].

The anthropomorphic breast model has been designed with a realistic three-dimensional (3-D) distribution of large- and medium-scale tissue structures, whose projections are visible in mammograms. The mammographic imaging process is simulated using a compression model and a model of the X-ray image acquisition process. Parameters controlling the size and placement of the simulated structures provide a method for consistently modeling images of the same initial breast composition with different simulated compression.

Using synthetic images generated from a 3–D breast model has an advantage that ground truth exists for the positions of the imaged anatomic structures, which is essential for the evaluation of registration methods. These ground truth positions are unavailable in clinical images; instead, readily identifiable objects are used for evaluation, [12], an approach which is sensitive to subjective errors (e.g., due to inaccuracy of manual identification, and the small number and limited extent of the objects).

The results derived from the use of synthetic images depend on the level of realism of the tissue and mammographic exam simulations. In our previous publications, we have evaluated similarity between synthetic and clinical images in terms of texture of mammogram parenchyma, [25] and the breast ductal network branching, [26], [27].

A. Three-Dimensional Anthropomorphic Breast Model

The uncompressed breast model has a shape defined by an ellipsoidal approximation of the breast outline and an ellipsoidal approximation of a border between internal regions with predominantly adipose tissue (AT) and predominantly fibroglandular tissue (FGT); these regions are regarded as the large-scale breast tissue structures [Fig. 1(a)]. The anatomic structures modeled within these tissue regions include skin, Cooper's ligaments, adipose tissue compartments within the AT and FGT regions, and the breast ductal network [Fig. 1(b)].

An analysis of subgross histological breast images and the corresponding mammograms showed that the background mammographic texture, or parenchymal pattern, is formed predominantly by the projection of connective tissue surrounding adipose tissue compartments, [24]. These compartments are included in the model to simulate the distribution of breast adipose tissue, and they form the medium-scale breast model elements, together with a model of the breast ductal network. The adipose tissue compartments are, as a first approximation, modeled as thin spherical shells in the AT region and small spherical blobs in the FGT region of the uncompressed model. The interiors of the shells and blobs have the elastic and X-ray attenuation properties of adipose tissue, while the shell layer and the portion of the FGT region surrounding the blobs simulate the properties of glandular and connective tissue. After simulating mammographic compression these compartments appear as ellipsoids. Generation of the simulated adipose compartments is described in more detail in the literature, [24].

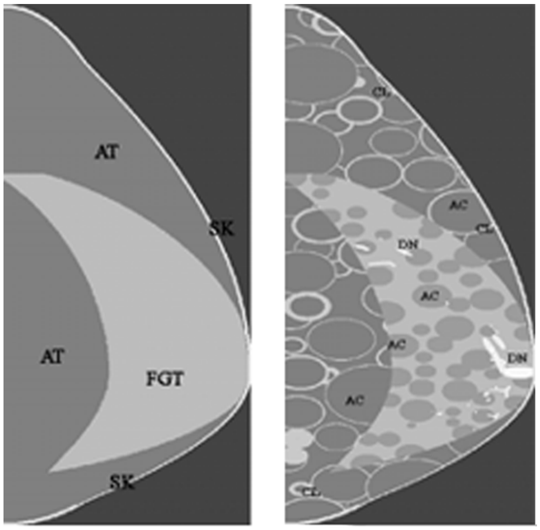

(a) (b)

Fig. 1. Cross section of the breast tissue model. (a) Simulated large-scale tissue structures: predominantly adipose tissue region (AT), predominantly fibroglandular tissue region (FGT), and skin (SK). (b) Simulated medium-scale internal anatomical structures: adipose compartments (AC), Cooper's ligaments (CL), and segments of the breast ductal network (DN).

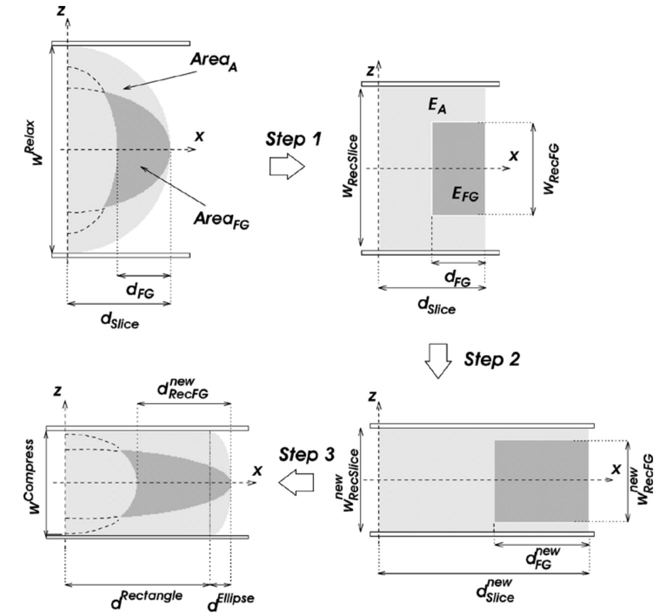

Fig. 2. Simulation of mammographic compression. Tissue deformation model is applied separately to each 1-voxel thick breast phantom slice, positioned orthogonally to the compression plates and chest wall. Step 1: A phantom slice is approximated by a composite beam. The beam contains two rectangular regions whose areas and centers of gravity correspond to the AT and FGT regions within the phantom slice. Step 2: The composite beam is elastically deformed based on the information about breast thickness before and after compression and the estimated elastic properties for the adipose and fibroglandular tissue types. Step 3: The deformed rectangular approximation is transformed into the slice of the compressed phantom, taking into account the flattened shape of the compressed breast.

B. Simulation of Mammographic Compression

Mammographic compression is simulated based upon tissue elasticity properties and a simplified breast deformation model. Deformation is simulated separately for each slice of the breast model. Each 1-voxel thick slice of the model, positioned orthogonally to the compression plates and chest wall, is approximated by a composite beam containing two rectangular regions corresponding to the sizes of the large-scale tissue regions within the slice. The composite beam is elastically deformed and then transformed into the flattened shape of a compressed breast with a thickness equal to the distance between the compression plates. Fig. 2 illustrates simulation of mammographic compression.

There is a significant variation in the values of tissue elasticity parameters found in the literature. There are many reasons for this variation, including differences in the measurement techniques and differences in the preparation of breast tissue samples. Moreover, the reported experimental measurements have most often been performed *in vitro* on small samples of different breast tissue types, while *in vivo* the elastic properties of the whole breast are also affected by the complex admixture of different breast tissues. We used parameters derived from the sound velocity in tissue, [28] and tissue density. Note that the values derived are unrelated to the values of γ and ν used in the registration algorithm, (3). Details of the compression simulation have been described in the literature, [24].

For simplicity, the X-ray image acquisition model used for generating synthetic mammograms in this study assumes a monoenergetic X-ray spectrum and a parallel beam geometry, without scatter, [24]. Using such a model, we have generated and analyzed synthetic medio-lateral oblique (MLO) mammographic views with various compressed breast thicknesses. Fig. 3(a) and (c) shows examples of synthetic projections of the same breast (i.e., the same initial distribution of simulated tissue structures,) for two different simulated compressed thicknesses.

IV. Evaluation

A. Protocol

Eleven breast tissue models were used for evaluating the registration methods. The dimensions of the AT and FGT regions (see Fig. 3, [24]) and the range of sizes of the spherical adipose compartments (4–10 mm in the AT region and 2–4 mm in the FGT region) were the same for all the models; however, each model had a different volumetric distribution of adipose compartments. Each model was synthetically compressed to four thicknesses (5, 6, 7, and 8 cm); the uncompressed breast thickness was 10 cm. All possible pairs of images generated from the same model with different compression thicknesses were registered using the methods described in Section II. Since the registration problem formulated in Section II is not symmetric, we distinguished registering an image A to an image B from registering an image B to an image A. As a consequence, twelve mammogram pairs were registered for each breast model.

The registration performance was measured by the average displacement error calculated over a number of evaluation points, identified in both the deformed source image and the target image. Three types of evaluation points were selected:

1) *AT/FGT border points*: Points at the projected 3-D border between the AT and FGT regions of the breast model (2358 points per image),
2) *FGT adipose compartment centers*: Points at the projected centers of adipose tissue compartments in the interior of the FGT region (357±10 points per image),

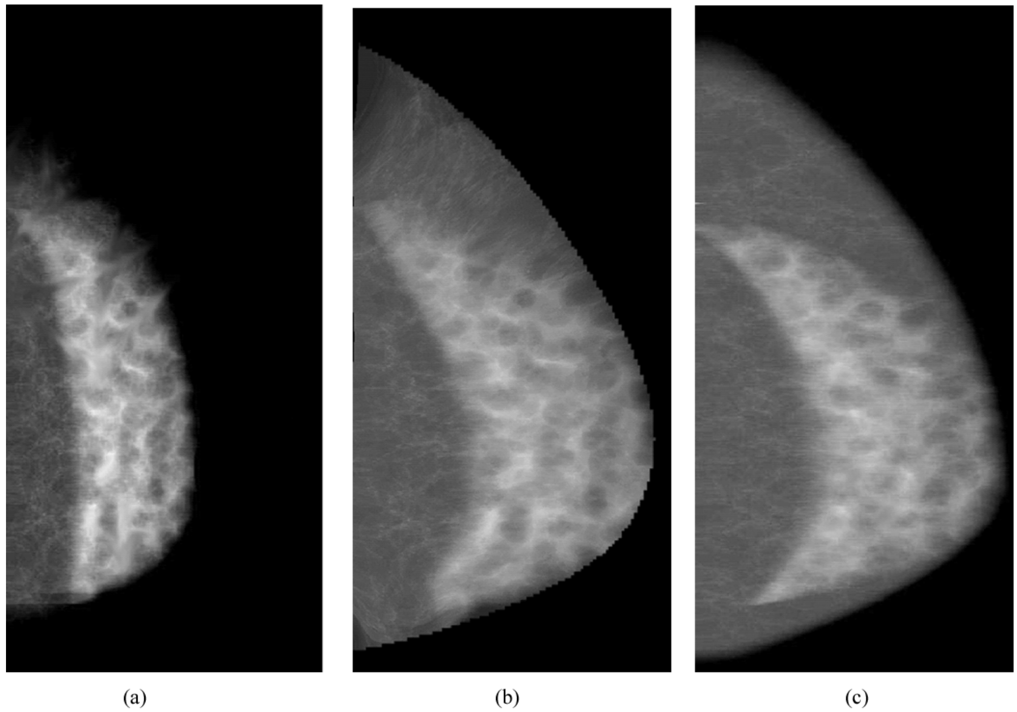

Fig. 3. Example of synthetic mammograms with the same initial internal composition. The model was compressed to (a) 8 cm (a) and (c) 5 cm . (b) Result of registering the 8-cm image with the 5-cm image.

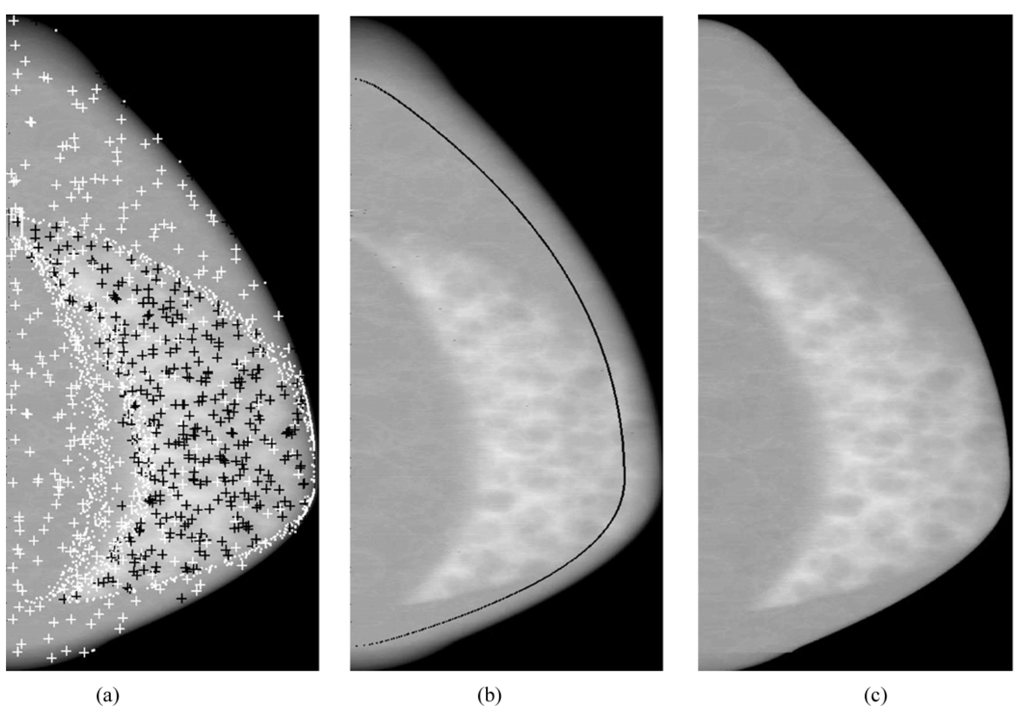

Fig. 4. (a) AT/FGT border points (bright dots), AT adipose compartment centers (bright crosses), and FGT adipose compartment centers (dark crosses). (b) The projected border (dark line) of the region with constant compressed breast thickness. (c) The thickness compensation applied to (b).

3) *AT adipose compartment centers*: Points at the projected centers of adipose tissue compartments in the interior of the AT region (343 ± 7 points per image).

An example of these types of evaluation points is shown in Fig. 4(a); the points are shown projected in the MLO view. These evaluation points are readily derived in the generation of the compressed breast model. Points of types 2) and 3) are uniformly distributed over the two tissue regions. We computed average displacement errors at different stages: before the registration, after the initial registration which is based only on border constraints and after the complete registration. Average displacement errors are reported in Table I.

In a preliminary study, [29], [30], we observed that the registration algorithm is adversely affected by thickness

TABLE I

AVERAGE DISPLACEMENT ERRORS AND STANDARD DEVIATIONS (IN MILLIMETERS) COMPUTED AT DIFFERENT STAGES OF THE NONRIGID REGISTRATION METHOD (BR, IR, CR), AND FOR AN AR. DATA ARE AVERAGED OVER ALL THE SYNTHETIC MAMMOGRAM PAIRS OF A GIVEN CD AND OVER DIFFERENT TYPES OF EVALUATION POINTS

AT/FGT border points						
CD	-1 cm	1 cm	-2 cm	2 cm	-3 cm	3 cm
BR	5.23±3.60	5.23±3.60	9.68±6.52	9.68±6.52	14.06±9.49	14.06±9.49
IR	1.89±1.67	1.75±1.54	2.38±2.05	2.16±1.82	3.29±2.73	2.80±2.24
CR	1.77±1.51	1.57±1.34	2.08±1.79	1.62±1.38	2.66±2.23	1.76±1.45
FGT adipose compartment centers						
CD	-1 cm	1 cm	-2 cm	2 cm	-3 cm	3 cm
BR	5.79±3.30	5.79±3.30	11.19±5.27	11.19±5.27	16.62±7.15	16.62±7.15
IR	1.81±1.60	1.64±1.42	2.17±1.73	2.07±1.58	2.84±2.27	2.96±2.05
CR	1.71±1.51	1.48±1.31	1.93±1.56	1.46±1.18	2.32±1.97	1.54±1.29
AT adipose compartment centers						
CD	-1 cm	1 cm	-2 cm	2 cm	-3 cm	3 cm
BR	3.11±2.70	3.11±2.70	6.15±5.10	6.15±5.10	9.35±7.56	9.35±7.56
IR	0.69±0.84	0.83±0.84	1.24±1.50	1.66±1.40	1.98±2.20	2.78±1.93
CR	0.78±1.03	0.77±1.02	1.46±1.70	1.30±1.55	2.49±2.62	2.01±2.11
all evaluation points						
CD	-1 cm	1 cm	-2 cm	2 cm	-3 cm	3 cm
BR	4.92 ± 3.50	4.92 ± 3.50	9.29 ± 6.24	9.29 ± 6.24	13.65 ± 9.01	13.65 ± 9.01
IR	1.63 ± 1.59	1.54 ± 1.45	2.11 ± 1.94	2.04 ± 1.71	2.94 ± 2.59	2.83 ± 2.15
CR	1.56 ± 1.48	1.39 ± 1.31	1.93 ± 1.74	1.52 ± 1.38	2.56 ± 2.27	1.77 ± 1.58
AR	2.27±2.12	2.27±2.12	3.89±3.75	3.89±3.75	5.78±5.17	5.78±5.17

CD=compression difference BR=before registration IR=initial registration *(border matching only)*
CR=complete registration AR=Affine registration

nonuniformity at the periphery of the compressed breast. We identified the image region in which the breast thickness is constant [Fig. 4(b), left of the dark line]; the average displacement errors computed over this region were much lower than those computed over the whole breast. We suspect this is an effect of the difference in pixel intensity over image regions with uniformly and nonuniformly compressed breast tissue. As a solution, we have applied a correction for thickness nonuniformity, by multiplying the pixel values by the ratio of the maximum compressed breast thickness to the thickness of the breast at the position of each pixel [see Fig. 4(c)]. We computed average displacement errors using such preprocessed images and showed that nonuniform thickness compensation improved the accuracy of registration by 14 percent, [29], [30]. This correction was applied to all images used in the current study. Thickness compensation could be applied to clinical mammograms using methods reported in the literature, e.g., by Snoeren *et al.*, [31] or by Rico *et al.*, [32].

The registration method presented in Section II consists of minimizing an energy term which contains a trade-off between regularization and similarity. This trade-off is controlled by the value of the regularization weighting factor, γ. We chose the value of γ using the L-curve approach developed for optimization of inverse problems, [33]. An L-curve is a graph of regularization scores, i.e., values of R in (1), versus similarity scores, i.e., values of S in (1), which are obtained by application of the algorithm as regularization weights vary. The L-curve which was obtained with the mammogram dataset is shown in Fig. 5. This L-curve shows a point of maximal curvature when the parameter value is approximately equal to 100. This optimal point separates the vertical part of the curve in which problem solutions are under-regularized and dominated by image noise from

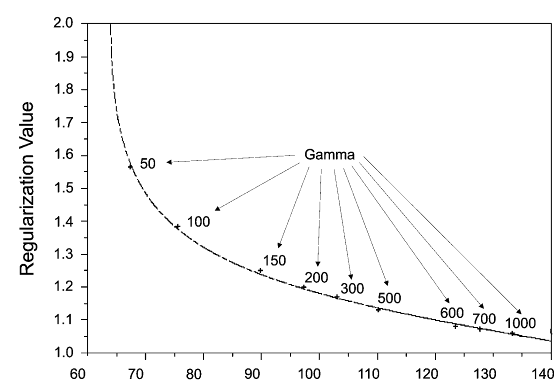

Fig. 5. Illustration of the optimization procedure used in the nonrigid registration method. Shown is an L-curve, a plot of the regularization versus similarity term (R and S in (1), respectively) calculated for different values of the weighting parameter γ. The optimum value of γ corresponds to the maximum curvature of the L-curve (here: $\gamma = 100$).

the horizontal part in which solutions are over-regularized. In the remaining experiments, $\gamma = 100$.

We have also compared the nonrigid registration results with those obtained using an optimal affine registration (AR), performed by fitting affine displacements to the displacements of all the evaluation points (see Section IV-A). Details about the method are given in Appendix B and the corresponding average displacement errors in Table I.

B. Results and Discussion

Table I summarizes the evaluation of the registration method, given in Section II, using synthetic image pairs generated as simulated mammographic projections through eleven breast tissue models. Average displacement errors and their standard deviations were computed over all synthetic mammogram pairs of a given compression difference (CD). The CD is defined as $\mathrm{CD} = T_{\mathrm{Source}} - T_{\mathrm{Target}}$, where T_{Source} is the compressed breast thickness corresponding to the source image and T_{Target} is for the target image. The results were computed using the three types of evaluation points (see Section IV-A) separately and combined. The average displacement errors are computed at three different stages. First, the displacement error is computed before the registration (BR). Next, an initial registration (IR) is obtained by taking into account only the constraints derived from the breast borders when solving the variational problem of (12) in Appendix A. The complete registration (CR) is obtained by also taking into account the intensity-based constraints.

The largest improvement observed after initial registration is for the highest CDs ($\mathrm{CD} = \pm 3$ cm); the displacement errors decrease from 13.7 mm (BR) to 2.8–2.9 mm (IR) when averaged over all the evaluation points. Even when registering images with the smallest analyzed CDs ($\mathrm{CD} = \pm 1$ cm), the errors are substantially reduced after the initial registration, dropping from 4.9 mm (BR) to 1.5–1.6 mm (IR). After the complete registration (CR), the average displacement error is further reduced to 1.8–2.6 mm for $\mathrm{CD} = \pm 3$ cm, and 1.4–1.6 mm for $\mathrm{CD} = \pm 1$ cm.

The optimal AR method results in statistically significantly $(\mathrm{p} < 0.05)$ larger registration errors than the CR method, e.g., 3.9 mm (AR) versus 1.5–1.9 mm (CR), for $\mathrm{CD} = \pm 2$ cm. The registration error of the AR method was dependent upon the CD value; the CR method showed little dependence upon the breast thickness difference (the ratio of the registration errors between the AR and CR methods increases from 1.5 to 2.7 for CD values of 1–3 cm). Note, however, that the AR method is not sensitive to the ordering of the registered images.

We observed that the registration performance depended upon the order of the registered images. The registration error is lower when the amount of compression used for the source image is lower (i.e., the compressed breast thickness is higher) than for the target image, which corresponds to positive CD values in Table I. For example, the registration error is 1.5 mm for $\mathrm{CD} = 2$ cm, while the error is 1.9 mm for $\mathrm{CD} = -2$ cm.

We do not yet have a definitive explanation for this observation. However, one plausible reason is proposed. Let us denote by Φ_S and Φ_T the 3-D maps from the uncompressed breast volume onto the source and target compressed breast volumes, respectively. Further, let us denote by ϕ_S and ϕ_T the 2-D image maps from a projection of the uncompressed breast onto the source and target registration images, respectively. The volume map from the source onto the target compressed breast volume can be expressed as $\Phi_T \circ \Phi_S^{-1}$, where Φ_S^{-1} represent the inverse 3-D map from the source compressed breast onto the uncompressed breast volume. The solution to the mammogram registration problem may be expressed as the 2-D map from the source image onto the target image, $\phi_T \circ \phi_S^{-1}$; this assumes that the inverse transform from the source image to the projection image of the uncompressed breast ϕ_S^{-1} exists. Note that although both 3-D maps Φ_S and Φ_T are invertible, there is no guarantee that ϕ_T and ϕ_S are. The assumption of invertibility is more likely to be violated when the source image has been acquired with the greater compression. This is consistent with our observation that higher registration errors occur in cases with negative CD values (see Table I). Fig. 6 illustrates this observation for the example of breasts compressed to 5 and 8 cm.

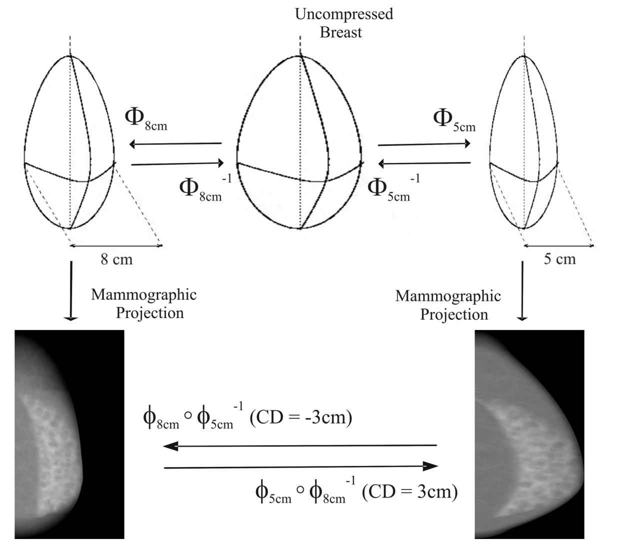

Fig. 6. Registration performance is dependent upon the order of the registered images. $\Phi_{5\ \mathrm{cm}}$ and $\Phi_{8\ \mathrm{cm}}$ are the 3-D maps from the uncompressed breast volume onto the breast volumes compressed to 5 and 8 cm, respectively. The corresponding 2-D image maps, from a projection of the uncompressed breast onto the mammograms of the 5- and 8-cm-thick compressed breasts, are labeled by $\phi_{5\ \mathrm{cm}}$ and $\phi_{8\ \mathrm{cm}}$, respectively. The solution to the problem of registering the 5-cm image onto the 8-cm image can be expressed as the 2-D map $\phi_{8\ \mathrm{cm}} \circ \phi_{5\ \mathrm{cm}}^{-1}$, assuming that the inverse map $\phi_{5\ \mathrm{cm}}^{-1}$ exists. For such registration image pairs, corresponding to $\mathrm{CD} = -3$ cm in Table I, we observed that the average registration error is 2.6 mm. Similarly, the registration of the 8 cm onto the 5-cm image can be expressed by the map $\phi_{5\ \mathrm{cm}} \circ \phi_{8\ \mathrm{cm}}^{-1}$, assuming that the inverse map $\phi_{8\ \mathrm{cm}}^{-1}$ exists. Such registration pairs correspond to $\mathrm{CD} = 3$ cm in Table I, with an observed average registration error of 1.6 mm. This example illustrates our hypothesis that registration is superior for positive values of CD.

In order to validate the chosen range of simulated CDs, we performed a retrospective study of 143 mammographic exams obtained from 30 patients imaged at the Hospital of the University of Pennsylvania and five other Philadelphia area hospitals between July 1996 and March 2005. We calculated the mean and standard deviation of the compressed breast thickness for each mammographic view (mediolateral-oblique, MLO, or craniocaudal, CC), for each breast, [34]. The root-mean-square value of the standard deviations is 0.71 cm. Assuming a normal distribution of compressed breast thickness differences, 96 percent of clinical CD values are expected to fall within four standard deviations ($\pm 2\sigma$), which is equal to 2.84 cm on average for all four views. The maximum observed per-patient CD value was 3.3 cm averaged over all four mammographic views. The analyzed range of CDs in synthetic mammograms, CD $\in (-3, 3)$ cm, is comparable with the clinically observed range.

V. Conclusion

The registration method described in Section II was successfully applied to synthetic mammograms with varying amounts of compression. The evaluation results show that the nonrigid technique can be considered as being robust to accurately correcting breast CDs. We observed that the registration method is affected by the order of images in mammogram pairs. The amount of breast compression is usually measured during the mammographic exam; sometimes, it can be estimated from mammograms, [35]. We suggest selecting the image with less compression as the registration source image. From our previous work [29], [30] we note that it is necessary to apply nonuniform thickness compensation. The resulting nonrigid registration method yields an average displacement error of approximately 1.6 mm. By comparison the optimum AR method results in an average displacement error of approximately 4.0 mm.

This paper is the first step of a long-term project to develop a complete evaluation platform for the comparison of mammogram registration methods. Registration method design involves making assumptions about the nature of observed image variations (e.g., underlying deformations, image gray-level dependencies), choosing an optimization approach (e.g., variational, [14] or Markovian approach, [36]), and adopting an implementation strategy (e.g., finite elements). An evaluation platform is essential to test the validity of all aspects of a registration methods. Such a platform is available for brain imaging [37], but none exist for breast imaging.

The trend in clinical breast imaging is toward the integration of different modalities (e.g., mammography, breast MRI, breast ultrasound, breast PET, contrast-enhanced mammography, [5], tomosynthesis, [38], [39]). These modalities are based on different physical properties (e.g., X-ray attenuation coefficient in mammography versus proton density in MRI), and are acquired under different conditions (i.e., positioning and compression, resolution, and dimensionality of data). Such modality variations require development of appropriate registration methods, and an adequate evaluation approach. In this context, we believe that our breast model-based evaluation strategy is of particular importance, since it allows simulation of different imaging modalities applied to the same synthetic breast anatomy.

There are two aspects to evaluating the performance of medical image registration methods: technical efficacy in correcting variations between images from a registration pair, and diagnostic efficacy in detecting cancer at the earliest stage possible. This paper focuses on an approach to evaluate technical performance of mammogram registration techniques by separately analyzing effects of one specific cause of image variations, namely changes in compressed breast thickness. In our future research, we plan to extend the same approach to analysis of other breast compression related effects (e.g., shear and rotation), as well as the effects of tissue composition and the occurrence of abnormalities. Phantom-based evaluation of registration performance allows separation of the causes of image variations of interest in synthetic mammograms. On the other hand, diagnostic performance of registration requires a clinical study in which radiologists are asked to identify abnormalities in blinded sets of mammograms with and without registration applied. We believe that such studies should occur after the technical accuracy of registration has been confirmed.

Appendix A
Nonrigid Registration Algorithm

We present here a technique for the numerical solution of the problem in (10).

A. Algorithm Principles

We have designed a gradient descent algorithm (GD) for the numerical solution of the problem in (10).

Let us denote by $\mathcal{W}'_0$ the subspace of $\mathcal{W}'$ which is composed of the functions of $\mathcal{W}'$ equal to 0 on $\partial\Omega_0$. Let δ_0 be the solution in $\mathcal{W}'_0$ of the linear variational equations

$$\forall v \in \mathcal{W}_0, \quad A_{\Omega_0}(\delta, v) + A_{\Omega_0}(u_0, v) = 0. \tag{12}$$

First, note that functions $u \in \mathcal{W}'$ which are consistent with boundary conditions in (11) are of the form $u = \tilde{u} + \delta_0 + u_0$, where $\tilde{u} \in \mathcal{W}'_0$. Hence, minimizing the energy $J_{\Omega_0}(u)$ over $\mathcal{W}'$ with nonhomogeneous boundary conditions is equivalent to minimizing the energy $\tilde{J}_{\Omega_0}(\tilde{u}) = J(\tilde{u} + u_0 + \delta_0)$ over the subspace $\mathcal{W}'_0$.

Let us assume that the parameters g_1 and g_2 in $\tilde{J}_{\Omega_0}$ are known and fixed. The Fréchet-derivative of the energy $\tilde{J}_{\Omega_0}$ at point $\tilde{u} \in \mathcal{W}'_0$ in the direction $v \in \mathcal{W}'_0$ is given by

$$A_{\Omega_0}(\tilde{u}, v) - \langle f_{g_1,g_2}(\tilde{u} + \delta_0 + u_0), v \rangle_{\Omega_0} \tag{13}$$

where $f_{g_1,g_2}(u)$ is given by

$$f_{g_1,g_2}(u) = \left(g_1 I^0 + g_2 - I^1_{\mathrm{Id}+u}\right) \nabla I^1_{\mathrm{Id}+u}. \tag{14}$$

Thus, the gradient of energy $\tilde{J}_{\Omega_0}$ with respect to the inner product $A_{\Omega_0}(\cdot,\cdot)$ is of the form

$$\nabla \tilde{J}_{\Omega_0\,|\,\tilde{u}} = \tilde{u} - \delta_{g_1,g_2}(\tilde{u} + \delta_0 + u_0) \tag{15}$$

where $\delta_{g_1,g_2}(u)$ is the solution in $\mathcal{W}'_0$ of the linear equations: for all $v \in \mathcal{W}'_0$

$$A_{\Omega_0}(\delta, v) = \langle f_{g_1,g_2}(u), v \rangle_{\Omega_0}. \tag{16}$$

Next, using a time parameter $t \in \mathbb{R}^+$, it is possible to derive the GD algorithm. We denote by $u(t)$ successive approximations in $\mathcal{W}'$ of a local minimum of J. At each time t, we estimate the values $g_1(t) = \hat{g}_1(I^0, I^1_{\mathrm{Id}+u(t)})$ and $g_2(t) = \hat{g}_2(I^0, I^1_{\mathrm{Id}+u(t)})$, where functions $\hat{g}_1$ and $\hat{g}_2$ are defined by (7) and (8). Using previous gradient computations, we express the algorithm in terms of the following dynamic system:

$$u(0) = u_0 + \delta_0, \quad \text{and} \tag{17}$$

$$\forall\, t > 0, \quad \frac{du}{dt}(t) = \delta_{g_1(t),g_2(t)}(u(t)) \tag{18}$$

where at each time $t, \delta_{g_1(t),g_2(t)}(u(t))$ is the solution of (16).

B. Discretization

We discretized (12) and (16) using the Galerkin method, [40]. This method consist of approximating equations in a subspace $\mathcal{W}_0^h$ of $\mathcal{W}_0$ which is of a finite dimension h and spanned by a finite family $\{u_i^h\}_{i=1}^h$ of functions with compact support. The variational problem in (15) is approximated by variational equations

$$\forall v \in \mathcal{W}_0^h, \quad A_{\Omega_0}(\delta, v) = \langle f_{g_1,g_2}(u), v\rangle_{\Omega_0}. \tag{19}$$

The solution of these equations is of the form

$$\delta^h = \sum_{j\in I_h} \beta_j^h \psi_j^h \tag{20}$$

where the coefficients β_j^h are the solution of the linear system: for all $i \in \{1,\ldots,n\}$

$$\sum_{j\in I_h} \beta_j A_{\Omega_0}\left(u_j^h, u_i^h\right) = \left\langle f_{g_1,g_2}(u), u_i^h\right\rangle_{\Omega_0}. \tag{21}$$

In order to design the approximation spaces $\mathcal{W}_0^h$, the set Ω_0 is decomposed into $h/2$ fixed-size nonoverlapping squares. We define $\mathcal{W}_0^h$ as the space formed by the functions that are of class C^1 on Ω_0 and polynomial on each of the squares.

So as to reduce computation time and to obtain better minimization results, we also adopt a multigrid implementation approach together with a coarse-to-fine strategy. This approach is based on the definition of a series $\{\mathcal{W}_0^{h(k)}\}_{k=1}^K$ of K embedded subspaces

$$\mathcal{W}_0^{h(1)} \subset \cdots \subset \mathcal{W}_0^{h(k)} \subset \cdots \subset \mathcal{W}_0^{h(K)} \subset \mathcal{W}_0'.$$

The dynamic system in (17) and (18) is discretized with respect to time using the Euler method. After discretization, we obtain the following algorithm

Algorithm 1: Initialize $u(0)$ with $u_0 + \delta_0^{h(K)}$, where $\delta_0^{h(K)}$ is the solution in $\mathcal{W}_0^{h(K)}$ of (12).

In the kth iteration ($k \geq 0$), compute $u(k+1) = u(k) + \epsilon\delta(k)$, where ϵ is a small positive value and $\delta(k)$ is the solution in $\mathcal{W}_0^{h(k)}$ of (20) and (21) for $t = k, u = u(k), g_1 = g_1(k)$, and $g_2 = g_2(k)$.

Appendix B
Affine Registration Technique

Affine displacements are defined over points (x_1, x_2) of the domain Ω_1 as

$$u(x_1,x_2) = \begin{cases} u_1(x_1,x_2) = \alpha_1 x_1 + \alpha_2 x_2 + \gamma_1 \\ u_2(x_1,x_2) = \beta_1 x_1 + \beta_2 x_2 + \gamma_2 \end{cases}$$

where parameters $\alpha_1, \alpha_2, \beta_1$, and β_2 are scaling factors and γ_1 and γ_2 are translation factors. From a set of homologous fiducial points selected in the registration image pair, we derive indexed samples of true displacements $u^k = (u_1^k, u_2^k)$ at fiducial point positions $x^k = (x_1^k, x_2^k)$. We then fit affine displacements to these samples by computing the affine parameter values which minimize the mean square error

$$\mathrm{MSE} = \frac{1}{n}\sum_{k=1}^{n}\left(\alpha_1 x_1^k + \alpha_2 x_2^k + \gamma_1 - u_1^k\right)^2 + \frac{1}{n}\sum_{k=1}^{n}\left(\beta_1 x_1^k + \beta_2 x_2^k + \gamma_2 - u_2^k\right)^2$$

The explicit solutions of this problem are

$$\begin{aligned}
\alpha_1 &= \frac{\rho(x_1,u_1) - \frac{\rho(x_2,u_1)\rho(x_1,x_2)}{\sigma^2(x_2)}}{\sigma^2(x_1) - \frac{\rho(x_1,x_2)}{\sigma^2(x_2)}}\\
\alpha_2 &= \frac{\rho(x_2,u_1) - \alpha_1\rho(x_1,x_2)}{\sigma^2(x_2)}\\
\beta_1 &= \frac{\rho(x_1,u_2) - \frac{\rho(x_2,u_1)\rho(x_1,x_2)}{\sigma^2(x_2)}}{\sigma^2(x_1) - \frac{\rho(x_1,x_2)}{\sigma^2(x_2)}}\\
\beta_2 &= \frac{\rho(x_2,u_2) - \alpha_1\rho(x_1,x_2)}{\sigma^2(x_2)}\\
\gamma_1 &= \bar{u}_1 - \alpha_1\bar{x}_1 - \alpha_2\bar{x}_2\\
\gamma_2 &= \bar{u}_2 - \beta_1\bar{x}_1 - \beta_2\bar{x}_2
\end{aligned}$$

where, for real samples $f_1 = \{f_1^k\}_{k=1}^n$ and $f_2 = \{f_2^k\}_{k=1}^n$

$$\begin{aligned}
\bar{f}_1 &= \frac{1}{n}\sum_{k=1}^{n} f_1^k\\
\sigma^2(f_1) &= \frac{1}{n}\sum_{k=1}^{n}\left(f_1^k - \bar{f}_1\right)^2\\
\rho(f_1,f_2) &= \frac{1}{n}\sum_{k=1}^{n}\left(f_1^k - \bar{f}_1\right)\left(f_2^k - \bar{f}_2\right).
\end{aligned}$$

References

[1] F. Tavassoli, *Pathology of the Breast*, 2nd ed. Stamford, CT: Appleton & Lange, 1999.

[2] D. Kopans, *Breast Imaging*, 2nd ed. Philadelphia, PA: Lippincott, Williams & Wilkins, 1998.

[3] R. Highnam and J. Brady, *Mammographic Image Analysis*, ser. Kluwer series in Medical Imaging. Dordrecht, The Netherlands: Kluwer Academic Publishers, Mar. 1999.

[4] S. Astley *et al.*, "Automation in mammography: Computer vision and human perception," in *State of the Art in Digital Mammographic Image Analysis*. ser. Series in Machine Perception and Artificial Intelligence, K. W. Bowyer and S. Astley, Eds. Singapore: World Scientific, 1994, vol. 9, pp. 1–25.

[5] M. Skarpathiotakis *et al.*, "Development of contrast digital mammography," *Med. Phys.*, vol. 29, pp. 2419–2426, 2002.

[6] J. Lewin, P. Isaacs, V. Vance, and F. Larke, "Dual-energy contrast-enhanced digital subtraction mammography: Feasibility," *Radiology*, vol. 229, pp. 261–268, 2003.

[7] A.-K. Carton *et al.*, "Technical development of contrast-enhanced digital breast tomosynthesis," in Proc. 89th Scientific Assembly Annu. Meeting Radiological Society North America, 2005, to be published.

[8] A. Maidment and M. Albert, "Tissue discrimination methods in mammography," in *RSNA 2003 Syllabus. Advances in Digital Radiography*, E. Samei and M. Flynn, Eds, 2003, pp. 189–197.

[9] T. Lau and W. Bischof, "Automated detection of breast tumors using the asymmetry approach," *Comput. Biomed. Res.*, vol. 24, no. 3, pp. 273–295, 1991.

[10] J. Semmlow *et al.*, "A fully automated system for screening Xeromammograms," *Comput. Biomed. Res.*, vol. 13, pp. 350–362, 1980.

[11] A. Stamatakis *et al.*, "A novel approach to aligning mammograms," in *Proc. 2nd Int. Workshop Digital Mammography*, A. Gale *et al.*, Eds., July 1994, pp. 355–364.

[12] S. van Engeland, P. Snoeren, J. Hendriks, and N. Karssemeijer, "A comparison of methods for mammogram registration," *IEEE Trans. Med. Imag.*, vol. 22, no. 11, pp. 1436–1444, Nov. 2003.

[13] F. Richard and L. D. Cohen *et al.*, "A new image registration technique with free boundary constraints: Application to mammography," in *Proc. Eur. Conf. Computer Vision (ECCV)*, vol. 4, A. Heyden *et al.*, Eds., May 2002, pp. 531–545.

[14] F. Richard and L. Cohen, "Non-rigid image registration with free boundary constraints: Application to mammography," *J. Comput. Vis. Image Understanding (Special Issue on Nonrigid Registration)*, vol. 89, no. 2–3, pp. 166–196, 2003.

[15] M. Sallam and K. Bowyer *et al.*, "Detecting abnormal densities in mammograms by comparison to previous screenings," in *Proc. 3rd Int. Workshop on Digital Mammography*, K. Doi *et al.*, Eds., Jun 1996, pp. 417–420.

[16] ——, "Registration and difference analysis of corresponding mammogram images," *Med. Image Anal.*, vol. 3, no. 2, pp. 103–118, 1999.

[17] P. Bakic, M. Albert, D. Brzakovic, and A. Maidment, "Evaluation of a mammography simulation," in *Proc. 5th Int. Workshop Digital Mammography*, M. Yaffe, Ed., Jun 2000, pp. 681–687.

[18] P. Bakic, D. Brzakovic, P. Brzakovic, and Z. Zhu, "An approach to using a generalized breast model to segment digital mammograms," in *Proc. 11th IEEE Symp. Computer-Based Medical Systems*, Lubbock, TX, 1998, pp. 84–89.

[19] R. Novak, "Transformation of the female breast during compression at mammography with special reference to importance for localization of a lesion," Ph.D. dissertation, Dept. Diagnostic Radiol., Lakarhuset and Karolinska Sjukhuset, **<City?>**, Sweden, 1989.

[20] Y. Amit, "A nonlinear variational problem for image matching," *SIAM J. Scientif. Comput.*, vol. 15, no. 1, pp. 207–224, Jan. 1994.

[21] R. Bajcsy and S. Kovacic, "Multiresolution elastic matching," *CVGIP*, vol. 46, pp. 1–21, 1989.

[22] G. Christensen, R. Rabbitt, and M. Miller, "Mathematical textbook of deformable neuroanatomies," *Proc. Nat. Acad. Sci.*, vol. 90, pp. 11944–11948, Dec. 93.

[23] P. Ciarlet, *Mathematical Elasticity, Volume 1: Three-Dimensional Elasticity*, ser. Studies in Mathematics and its Applications. Amsterdam, The Netherlands: North-Holland, 1988.

[24] P. Bakic, M. Albert, D. Brzakovic, and A. Maidment, "Mammogram synthesis using a 3D simulation. I. Breast tissue model and image acquisition simulation," *Med. Phys.*, vol. 29, pp. 2131–2139, 2002.

[25] ——, "Mammogram synthesis using a 3D simulation. II. Evaluation of synthetic mammogram texture," *Med. Phys.*, vol. 29, pp. 2140–2149, 2002.

[26] P. Bakic, M. Albert, and A. Maidment, "Classification of galactograms using ramification matrices: Preliminary results," *Academic Radiol.*, vol. 10, pp. 198–209, 2003.

[27] P. Bakic, M. Albert, D. Brzakovic, and A. Maidment, "Mammogram synthesis using a 3D simulation. III. Modeling and evaluation of the breast ductal network," *Med. Phys.*, vol. 30, pp. 1914–1925, 2003.

[28] G. Kossoff, E. Fry, and J. Jellins, "Avarage velocity of ultrasouns in the human female breast," *J. Acoust. Soc. Am.*, vol. 53, pp. 1730–1736, 1973.

[29] P. Bakic, F. Richard, and A. Maidment, "Effect of breast compression on registration of successive mammograms," presented at the 7th Int. Workshop Digital Mammography, Chappel Hill, NC, Jun 2004.

[30] F. Richard, P. Bakic, and A. Maidment, "Non-rigid registration of mammograms obtained with variable breast compression: A phantom study," in *Lecture Notes in Computer Science*, vol. 2717, Proc. 2nd Workshop Biomedical Image Registration, J. Gee, Ed.. Philadelphia, PA, Jun 2003, pp. 281–290.

[31] P. Snoeren and N. Kerssemeijer, "Thickness correction of mammographic images by means of a global parameter model of the compressed breast," *IEEE Trans. Med. Imag.*, vol. 23, no. 7, pp. 799–806, Jul. 2004.

[32] D. Rico *et al.*, "Peripheral thickness correction for volumetric breast density estimation," in *Proc. 5th Int. Workshop Digital Mammography*, H.-O. Peitgen *et al.*, Ed.. Bremen, Germany, Jun. 2002, pp. 187–191.

[33] P. C. Hansen, "The L-curve and its use in the numerical treatment of inverse problems," in *Computational Inverse Problems in Electrocardiology*, ser. Advances in Computational Bioengineering. Southampton, U.K.: WIT Press, 2001, pp. 119–142.

[34] P. Bakic, Intra-patient variation of compressed breast thickness in mammography, in Phys. Med. Biol., 2005, submitted for publication.

[35] R. Highnam, J. Brady, and B. Shepstone *et al.*, "Estimating compressed breast thickness," in *Proc. 4th Int. Workshop Digital Mammography*, N. Karssemeijer *et al.*, Eds., June 1998, pp. 275–278.

[36] F. Richard, "The design of a markovian image matching technique and its comparison to variational technique in the context of mammogram registration," in *Proc. 1st IAPR-TC3 Conf. Artificial Neural Networks on Pattern Recognition*, M. Gori and S. Marinai, Eds., Florence, Italy, Sep. 2003, pp. 82–88.

[37] J. Fitzpatrick, J. West, and J. C. R. Maurer. (1998) Estimation of compressed breast thickness during mammography. *IEEE Trans. Med. Imag.* [Online], pp. 694–702. Available: http://www.vuse.vanderbilt.edu/~image/registration/

[38] L. Niklason *et al.*, "Digital tomosynthesis in breast imaging," *Radiology*, vol. 205, pp. 399–406, 1997.

[39] A. Maidment, M. Albert, and E. Conant, "Three-dimensional imaging of breast calcifications," *Proc. SPIE*, vol. 3240, pp. 200–208, 1998.

[40] P. G. Ciarlet, *The Finite Element Method for Elliptic Problems*. Amsterdam, The Netherlands: North-Holland, 1978.